THE JOURNAL OF BIOLOGICAL CHEMISTRY VOL. 289, NO. 5, pp. 2632–2642, January 31, 2014

A C4-oxidizing Lytic Polysaccharide Monooxygenase Cleaving Both Cellulose and Cello-oligosaccharides*

Received for publication, October 28, 2013, and in revised form, December 3, 2013 Published, JBC Papers in Press, December 9, 2013, DOI 10.1074/jbc.M113.530196

Trine Isaksen[‡], Bjørge Westereng[‡§], Finn L. Aachmann[¶], Jane W. Agger[‡], Daniel Kracher[‖], Roman Kittl[‖], Roland Ludwig[‖], Dietmar Haltrich[‖], Vincent G. H. Eijsink[‡1], and Svein J. Horn[‡]

From the [‡]Department of Chemistry, Biotechnology and Food Science, Norwegian University of Life Sciences, N-1432 Ås, Norway, [§]Forest and Landscape, University of Copenhagen, DK-1958 Frederiksberg C, Denmark, the [¶]Department of Biotechnology, NOBIPOL, Norwegian University of Science and Technology, N-7491 Trondheim, Norway, and the [‖]Department of Food Science and Technology, BOKU, University of Natural Resources and Life Sciences, A-1190 Vienna, Austria

Background: Lytic polysaccharide monooxygenases (LPMOs) are recently discovered enzymes that cleave polysaccharides.
Results: We describe a novel LPMO and use a range of analytical methods to characterize its activity.
Conclusion: Cellulose and cello-oligosaccharides are cleaved by oxidizing the sugar at the nonreducing end in the C4 position.
Significance: This study provides unequivocal evidence for C4 oxidation of the nonreducing end sugar and demonstrates a novel LPMO substrate specificity.

Lignocellulosic biomass is a renewable resource that significantly can substitute fossil resources for the production of fuels, chemicals, and materials. Efficient saccharification of this biomass to fermentable sugars will be a key technology in future biorefineries. Traditionally, saccharification was thought to be accomplished by mixtures of hydrolytic enzymes. However, recently it has been shown that lytic polysaccharide monooxygenases (LPMOs) contribute to this process by catalyzing oxidative cleavage of insoluble polysaccharides utilizing a mechanism involving molecular oxygen and an electron donor. These enzymes thus represent novel tools for the saccharification of plant biomass. Most characterized LPMOs, including all reported bacterial LPMOs, form aldonic acids, *i.e.*, products oxidized in the C1 position of the terminal sugar. Oxidation at other positions has been observed, and there has been some debate concerning the nature of this position (C4 or C6). In this study, we have characterized an LPMO from *Neurospora crassa* (*Nc*LPMO9C; also known as NCU02916 and *Nc*GH61–3). Remarkably, and in contrast to all previously characterized LPMOs, which are active only on polysaccharides, *Nc*LPMO9C is able to cleave soluble cello-oligosaccharides as short as a tetramer, a property that allowed detailed product analysis. Using mass spectrometry and NMR, we show that the cello-oligosaccharide products released by this enzyme contain a C4 gemdiol/keto group at the nonreducing end.

In the emerging bio-economy, plant biomass will gradually substitute fossil resources for the production of fuels, chemicals, and materials. One of the main bottlenecks in such biorefining processes is the depolymerization of cellulose, a major constituent of the plant cell wall, to fermentable sugars. In nature this process is catalyzed by cellulases and the recently discovered lytic polysaccharide monooxygenases (LPMOs)[2] (1). Enzymes and binding domains interacting with polysaccharides are categorized in the CAZy database, which comprises families of structurally related carbohydrate-active enzymes, such as glycoside hydrolases (GH), and carbohydrate-binding modules (CBMs) (2). LPMOs were originally classified as CBM33 (family 33 carbohydrate-binding module) or GH61 (family 61 glycoside hydrolase). However, CAZy has recently been revised, and GH61 and CBM33 are now named LPMOs and classified under the heading "auxiliary activities" (AA) as families AA9 and AA10, respectively (3).

The enzyme activities of LPMOs were first discovered in 2010 for an AA10 protein (CBP21) acting on chitin (4). Following this study, cellulose active LPMOs were found in both the AA10 (5) and AA9 (6–8) families. These copper-dependent enzymes carry out oxidative cleavage of the β-1,4-glycosidic bonds in polysaccharides, using molecular oxygen and an electron donor (1). Electrons may be supplied by small molecule reductants such as ascorbic acid and gallic acid (4, 6) or by enzymes, such as cellobiose dehydrogenase (CDH), that are co-

* This work was supported by Norwegian Research Council Projects 193817, 203402, 214613, 216162, and 217708 and by the European Commission through the FP7-KBBE-2013-7-613549 project INDOX.

[1] To whom correspondence should be addressed: Department of Chemistry, Biotechnology, and Food Science, The Norwegian University of Life Sciences, 1432 Ås, Norway. Tel.: +47 64965892; Fax: +47 64965901; E-mail: vincent.eijsink@nmbu.no.

[2] The abbreviations used are (full IUPAC abbreviations in bold type for clarity): LPMO, lytic polysaccharide monooxygenase; CBM, carbohydrate-binding module; GH, glycoside hydrolase; AA, auxiliary activities; DP, degree of polymerization; CDH, cellobiose dehydrogenase; PASC, phosphoric acid swollen cellulose; HPAEC, high performance anion exchange chromatography; DQF-COSY, double quantum filter correlation spectroscopy; IP-COSY, in-phase COSY; TOCSY, total correlation spectroscopy; HSQC, heteronuclear single quantum coherence; HMBC, heteronuclear multibond correlation; Glc4gemGlc, 4-hydroxy-β-D-*xylo*-hexopyranosyl-(1→4)-β-D-glucopyranosyl, **4-hydroxy-β-D-*xylo*-Hex*p*-(1→4)-β-D-Glc*p***; Glc4KGlc$_2$, β-D-*xylo*-hexos-4-ulopyranosyl-(1→4)-β-D-glucopyranosyl-(1→4)-β-D-glucopyranosyl, **β-D-*xylo*-Hex4ulo*p*-(1→4)-β-D-Glc*p*-(1→4)-β-D-Glc*p***; Glc4gemGlc$_2$, 4-hydroxy-β-D-*xylo*-hexopyranosyl-(1→4)-β-D-glucopyranosyl-(1→4)-β-D-glucopyranosyl, **4-hydroxy-β-D-*xylo*-Hex*p*-(1→4)-β-D-Glc*p*-(1→4)-β-D-Glc*p***; Glc4KGlcGlc1A, β-D-*xylo*-hexos-4-ulopyranosyl-(1→4)-β-D-glucopyranosyl-(1→4)-D-gluconic acid, **β-D-*xylo*-Hex4ulop-(1→4)-β-D-Glc*p*-(1→4)-D-Glc1A**; Glc4gemGlcGlc1A, 4-hydroxy-β-D-*xylo*-hexopyranosyl-(1→4)-β-D-glucopyranosyl-(1→4)-D-gluconic acid, **4-hydroxy-β-D-*xylo*-Hex*p*-(1→4)-β-D-Glc*p*-(1→4)-D-Glc1A**.

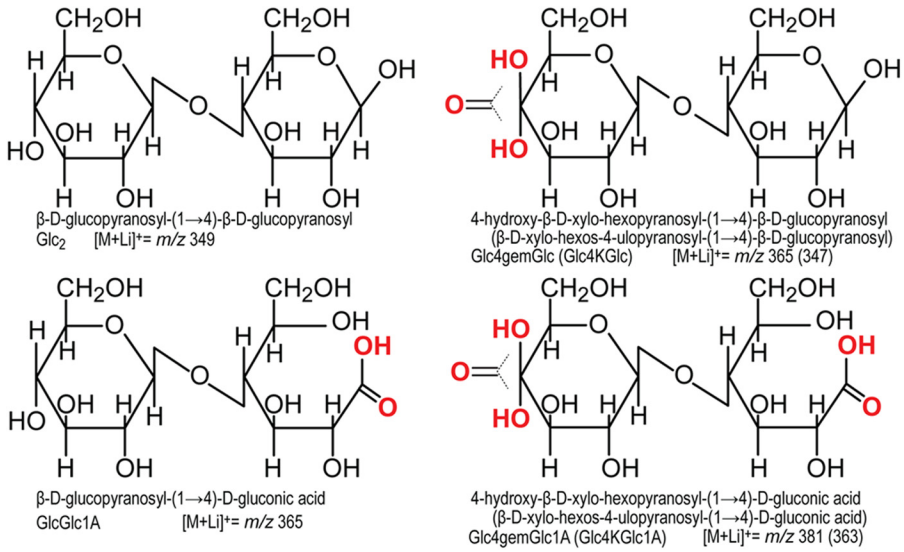

FIGURE 1. **Overview of cellobiose with C1 and/or C4 oxidations.** Oxidations are shown in red. The IUPAC names, the abbreviations, and the *m/z* values for lithium adducts are provided below the structures (please see Table 1 for a complete list of other adducts). In the *right two structures*, the IUPAC name, the abbreviation, and the *m/z* of the lithium adduct for the keto-form are given in *parentheses*.

expressed with LPMOs (8–10). The products of the reaction are oxidized oligosaccharides and native oligosaccharides containing reducing ends originally present in the polymeric substrate (1, 7) (Fig. 1). Although cleavage of polysaccharides by C1 oxidizing LPMOs, which yields aldonic acids, has been thoroughly demonstrated and analyzed (4, 5, 7, 8, 11, 12), oxidation at the nonreducing end is more difficult to analyze. Based on mass spectrometry, both oxidation at C4 and C6 have been suggested (6, 8, 13). For products generated by *Nc*LPMO9D (also known as NCU01050 or *Nc*GH61–4), oxidation at C4 rather than at C6 has been shown indirectly by detection of the C4 epimer of glucose, galactose, upon reduction of reaction products and by the absence of glucuronic acid upon hypoiodite oxidation of reaction products (14). However, direct evidence for the identity of the nonreducing end oxidized species is lacking.

The filamentous ascomycete *Neurospora crassa* is an efficient degrader of plant cell walls and produces a wide range of LPMOs and hydrolytic enzymes. The genome of *N. crassa* is predicted to contain 14 AA9 family LPMOs, six of which are attached to a CBM1 carbohydrate-binding module (15). These CBM1 modules contain ~40 amino acids, typically bind cellulose, and are almost exclusively found in fungi. The activities of three of these LPMOs on cellulose have been qualitatively characterized by HPLC and MS analyses of released products. *Nc*LPMO9E (NCU08760, *Nc*GH61–5; attached to a CBM1) oxidizes C1, *Nc*LPMO9D exclusively oxidizes the nonreducing end, and *Nc*LPMO9M (NCU07898, *Nc*GH61–13) seems to be capable of oxidizing both C1 and the nonreducing end (8, 16). In another study, using CDH as an electron donor, it was shown that three additional *N. crassa* AA9s, *Nc*LPMO9C (NCU02916, *Nc*GH61–3; attached to a CBM1), *Nc*LPMO9F (NCU03328, *Nc*GH61–6), and *Nc*LPMO9J (NCU01867, *Nc*GH61–10; attached to a CBM1), degrade cellulose, but no attempts were made to unravel details of the reaction products of these enzymes (17).

In this study, we have characterized the activity of *Nc*LPMO9C using NMR, mass spectrometry, HPLC, and a previously described activity assay (17). Interestingly, *Nc*LPMO9C turned out to be active on soluble substrates, which is an activity not previously described for LPMOs. Exploiting this unique property, we used NMR analysis to identify the products generated by *Nc*LPMO9C.

EXPERIMENTAL PROCEDURES

Production and Purification of Enzymes—The AA9 encoding *N. crassa* gene NCU02916 was codon-optimized, cloned with its native signal sequence under control of the methanol inducible AOX1 promotor, and recombinantly produced in *Pichia pastoris* X-33 following a published protocol (10). The protein was purified from 0.4 liter of culture supernatant by three subsequent chromatographic steps following a published method (17). In total, 28 mg of purified *Nc*LPMO9C was obtained, and the homogeneity was verified by SDS-PAGE. Cellobiose dehydrogenase from *Myriococcum thermophilum* carrying a C-terminal CBM1 (*Mt*CDH, Uniprot accession number A9XK88) (18) was recombinantly expressed in *P. pastoris* using methanol for induction (19). The enzyme was purified from 1 liter of culture supernatant by two chromatographic steps according to the procedure described by Harreither *et al.* (20), and 180 mg of homogeneous *Mt*CDH was obtained.

Activity Assays—Standard reaction mixtures (100–300 μl of liquid volume) contained the substrate (0.4 mg/ml cello-oligosaccharide degree of polymerization (DP) 3–6; (Megazyme), 1 mg/ml phosphoric acid swollen cellulose (PASC prepared from Avicel as described by Wood (21), 2.5 mg/ml Avicel PH-101 (Fluka) or (0.15–0.30 mg/ml) steam-exploded spruce), 4.4–8.8 μM *Nc*LPMO9C, 5 mM ammonium acetate buffer, pH 6.0, and 2 mM reducing agent (hydroquinone, ascorbic acid, or catechin; all from Sigma-Aldrich). In some reactions, the reducing agent was replaced by 1.4 μM *Mt*CDH. Additional substrates tested under the same conditions were: maltodextrin (DP4–14; Glu-

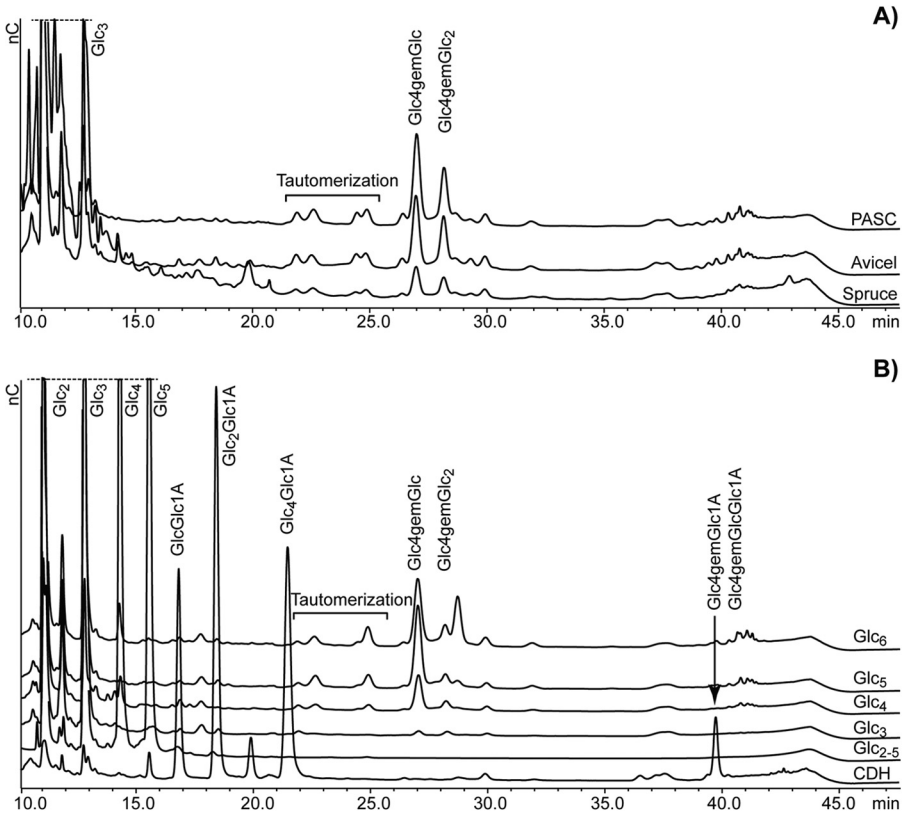

FIGURE 2. **Degradation of cellulose and cello-oligosaccharides by *Nc*LPMO9C.** *A* shows overlaid HPAEC chromatograms of oligosaccharides released upon degradation of 1 mg/ml of PASC, Avicel, and steam-exploded spruce with 8.8 μM *Nc*LPMO9C. *B* shows products released upon incubation of 0.4 mg/ml cello-oligosaccharides with 4.4 μM *Nc*LPMO9C (Glc_n traces), a standard mixture of nonoxidized cello-oligosaccharides (DP2–5, Glc_{2-5} trace), as well as products released upon incubation of cellopentaose with 4.4 μM *Nc*LPMO9C and 1.4 μM *Mt*CDH (CDH trace). All reaction mixtures contained 2 mM ascorbic acid (except the one containing CDH) and 5 mM ammonium acetate buffer, pH 6.0, and were incubated for 24 h at 50 °C. Reactions with insoluble substrates were incubated with horizontal shaking at 850 rpm. For product nomenclature, see Fig. 1. See text for further details.

cidex 9 from Roquette) mannohexaose, xylopentaose, xylohexaose, chitopentaose (all from Megazyme), α-chitin from shrimp shell (HovBio, Tromsø, Norway), and nanofibrillar α-chitin and β-chitin (10–20 nm) (22). All reactions were incubated in 2-ml screw cap microtubes (Sarstedt) at 50 °C in an Eppendorf Thermo mixer with (for insoluble substrates, 850 rpm) or without (for soluble substrates) shaking.

HPLC Analysis—From the standard reactions, samples were taken at different time points, and the reaction was stopped by adding NaOH to a final concentration of 0.05 M. After removing insoluble substrates by centrifugation, the supernatant was centrifuged and analyzed by high performance anion exchange chromatography (HPAEC) using an ICS3000 system (Dionex, Sunnivale, CA) as described previously (12). In brief, a 2-μl sample was injected on a CarboPac PA1 2 × 250 mm analytical column (Dionex) coupled to a CarboPac PA1 2 × 50 mm guard column kept at 30 °C. Cello-oligosaccharides were eluted at 0.25 ml/min using a stepwise linear gradient from 100% eluent A (0.1 M NaOH) toward 10% eluent B (1 M NaOAc in 0.1 M NaOH) 10 min after injection and 30% eluent B 25 min after injection, followed by a 5 min exponential gradient to 100% B. The column was reconditioned between each run by running initial conditions for 9 min.

Analysis by Mass Spectrometry—For time resolved product analysis, electrospray ionization mass spectrometry (ESI-MS) was used with a linear ion trap LTQ Velos Pro (Thermo Scientific, San Jose, CA USA) coupled to an UltiMate 3000 RS UHPLC from Dionex (Sunnyvale, CA USA) which delivered a constant flow and performed injection. No chromatographic separation was employed. The UHPLC delivered a flow of 0.2 ml/min of 30/70 (v/v) H_2O and acetonitrile via the auto-sampler. Standard reaction mixtures were incubated in the thermostatted auto-sampler of the UHPLC at 15 °C during the entire reaction time and samples of 2 μl were injected at given time points. The electrospray was operated in positive mode at 4 kV spray current, with a sheath gas flow of 30 (arbitrary units), an auxiliary gas flow of 5 (arbitrary units) and a capillary temperature of 250 °C. The acquisition time was set to 0.2 min with a data collection time of 10 ms per acquisition. Full scans were performed in the m/z 100–1000 mass range and fragmentation was done using higher energy collisional dissociation (HCD) with N_2 as the collision gas and normalized energy levels of 65, to enable observation of lower mass fragments. During fragmentation, data were collected in the m/z 100–400 mass range. The data were further processed using Xcalibur 2.2 SP1.48 (Thermo Scientific).

NMR Analysis—For NMR analysis, 1.0 mg/ml cellopentaose was dissolved in 99.996% D_2O (Cambridge Isotope Laboratories, Andover, MA) containing 5 mM sodium acetate (pD 6.0) and 0.1 ‰ (v/w) 3-(trimethylsilyl)-propionic-2,2,3,3-d4 acid sodium salt (Aldrich, Milwaukee, WI) used as chemical shift reference for proton and carbon. The NMR tubes contained

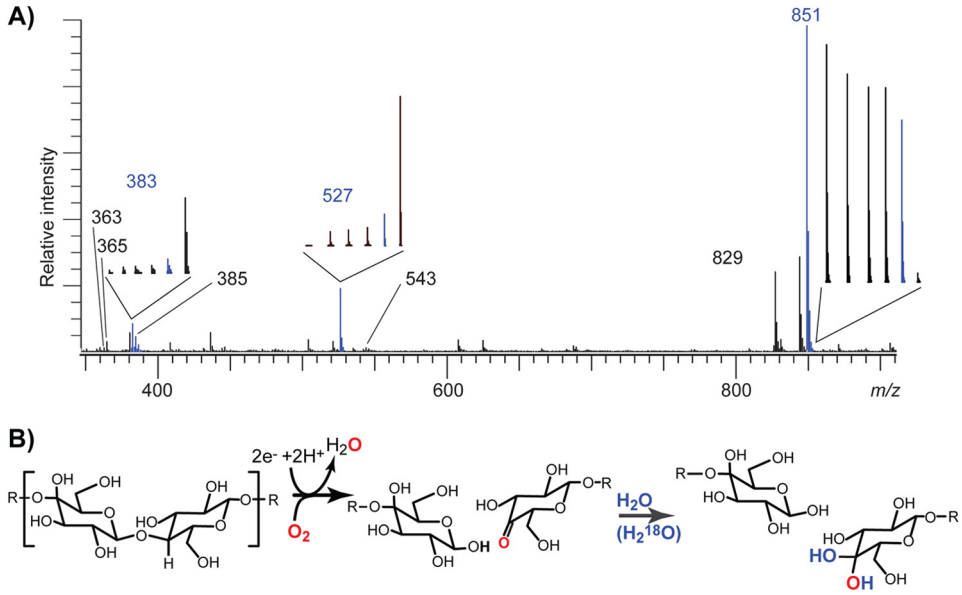

FIGURE 3. *A*, ESI-MS analysis of products generated over time during degradation of Glc_5 (*m/z* 851) in $H_2{}^{18}O$. Reaction products were analyzed after 0, 5, 15, 25, 90, and 1440 min of incubation, and the main picture shows the full spectrum for the 90-min sample. The *insets* show the signal over time for key products (from 0 to 1440 min, from *left* to *right*; the *blue* signal represents the 90-min sample). The *m/z* values 851, 527, and 365 correspond to the sodium adducts of Glc_5, Glc_3, and Glc_2, respectively (*m/z* 829 is $[M+H]^+$ for Glc_5), whereas *m/z* 383 and the minor *m/z* 543 correspond to $[M+Na]^+$ of gemdiol products (Glc4GemGlc and $Glc4GemGlc_2$) carrying one ^{18}O (see Fig. 1; the mass difference between sodium and lithium is 16 Da). The 383 signal is accompanied by a signal at *m/z* 385 because of exchange with the solvent, which gradually leads to incorporation of two ^{18}O atoms. The mass of 363 corresponds to the keto-form of the oxidized dimer ($[M+Na]^+$), and its intensity corresponds to ~10% of the intensity of the gemdiol. *B*, schematic presentation of enzymatic cleavage of the glycosidic bond and introduction of molecular oxygen in the nonreducing end, followed by water incorporation transforming the keto group into a gemdiol. The incorporation of water leads to uptake of ^{18}O in the products.

500 μl of cellopentaose stock solution and 33 μl of either *Mt*CDH (to a final concentration of 0.9 μM) or hydroquinone solution (to a final concentration of 3 or 10 mM). After addition of 17 μl *Nc*LPMO9C (to a final concentration of 2.9 μM), the head space of the NMR tube was flushed with pure oxygen gas (YARA, Trondheim, Norway) for ~10 s before sealing the tube. After incubation of the samples at 25 °C for 24 h, reaction products were analyzed with NMR spectroscopy.

All homo- and heteronuclear NMR experiments were recorded on a Bruker Avance 600 MHz NMR spectrometer (Bruker BioSpin AG, Fällanden, Switzerland) equipped with a 5-mm cryogenic CP-TCI z-gradient probe at 25 °C. For chemical shift assignment, the following spectra were recorded: one-dimensional proton, two-dimensional double quantum filter correlated spectroscopy (DQF-COSY), two-dimensional in-phase correlation spectroscopy (IP-COSY) (23), two-dimensional total correlation spectroscopy (TOCSY) with 70 ms of mixing time, two-dimensional ^{13}C heteronuclear single quantum coherence (HSQC) with multiplicity editing, two-dimensional ^{13}C HSQC-[^1H,^1H]TOCSY with 70 ms of mixing time on protons, and two-dimensional heteronuclear multibond correlation (HMBC) with BRID filter to suppress first order correlation. The NMR data were processed and analyzed with TopSpin 2.1 and TopSpin 3.0 software (Bruker BioSpin).

H_2O_2 Analysis—A fluorimetric assay based on Amplex Red and horseradish peroxidase (17) was used to measure the extent of H_2O_2 generation, which is a futile side reaction catalyzed by the reduced LPMO copper center. The peroxidase catalyzed conversion of Amplex Red to resorufin is proportional to H_2O_2 production (stoichiometry = 1). The increase of fluorescence was measured with an Enspire Multimode plate reader (PerkinElmer Life Sciences) using an excitation wavelength of 569 nm and an emission wavelength of 585 nm. The well plate assay (total volume of 200 μl, 30 °C, 6 min) was performed in 100 mM potassium phosphate buffer, pH 6.0, containing 50 μM Amplex Red, 7.1 units ml^{-1} horseradish peroxidase, 0.87 μM LPMO, and 30 μM ascorbate as reductant in 100 mM sodium phosphate buffer, pH 6.0. Cello-oligosaccharides (DP2–6; Sigma-Aldrich) were added to a final concentration of 5 mM.

Sequence Alignment and Modeling—A structure-guided sequence alignment to compare *Nc*LPMO9C with two structurally characterized AA9-type LPMOs, *Nc*LPMO9D (NCU01050; Protein Data Bank code 4EIR), and *Pc*LPMO9D (*Pc*GH61D; Protein Data Bank code 4B5Q), was constructed using the Expresso mode of the T-Coffee multiple sequence alignment server (24). A homology model of *Nc*LPMO9C was made based on a structure prediction by HHpred (25) and by using Modeler (26) with the crystal structure of *Nc*LPMO9D as a template. All structural comparisons were carried out using PyMOL (PyMOL Molecular Graphics System, version 1.5.0.4; Schrödinger, LLC). The coordinates for cellopentaose were derived from Protein Data Bank entry 2EEX (27).

RESULTS AND DISCUSSION

Enzyme Activity on Cellulose and Cello-oligosaccharides—Initial activity screening of the enzyme was done with a well established HPAEC method for the detection of C1-oxidized cello-oligosaccharide products (12). Incubation of *Nc*LPMO9C with polymeric substrates (PASC, Avicel, steam-exploded spruce; Fig. 2*A*) showed release of soluble cello-oligosaccharides (DP2 and DP3), but C1 oxidized species were not detected. Instead, two dominant later eluting peaks (between

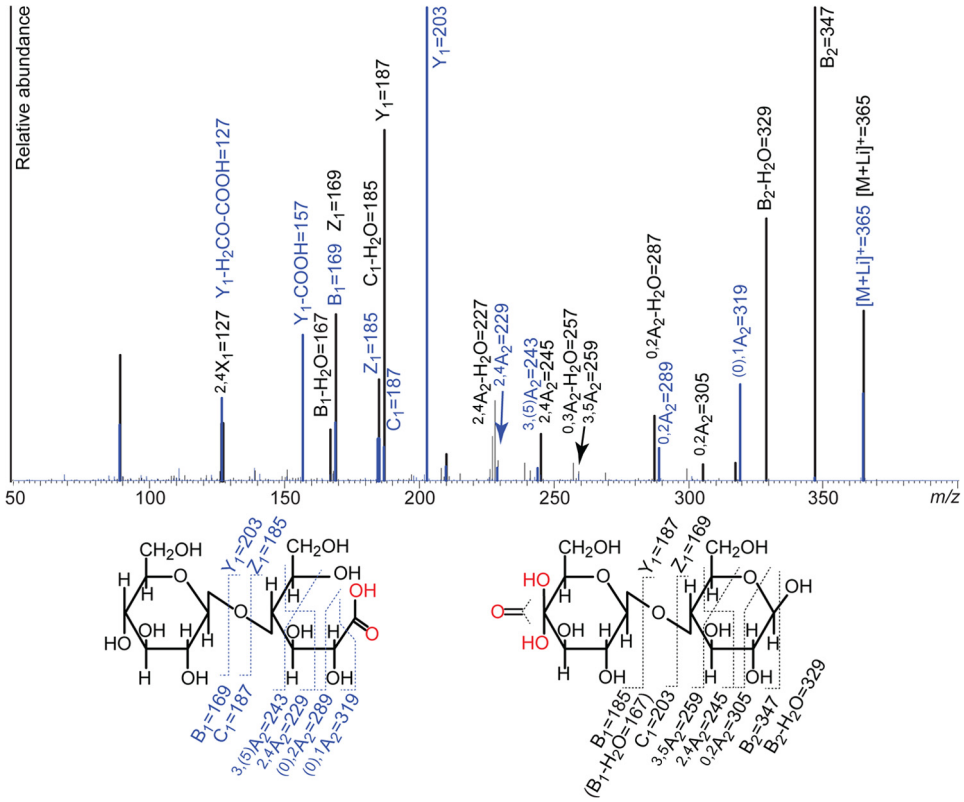

FIGURE 4. **MS/MS analysis of reaction products.** The picture shows overlaid MS/MS spectra obtained for the cellobionic acid generated by *Pc*LPMO9D (*left structure*; *blue trace* and *labeling*) and the oxidized dimer from an *Nc*LPMO9C catalyzed reaction (*right structure*; *black trace* and *labeling*). The analysis was done with lithium doping and all labeled signals reflect lithium adducts.

26 and 29 min) were observed that could represent a different kind of oxidized product. Similar late eluting peaks have also been observed for PASC degradation by *Nc*LPMO9D (8). MS analysis (described in detail below) indicated that the later eluting of these two peaks represented a trimeric product, whereas the earlier peak represented a dimeric product.

Cellulose-active LPMOs characterized so far typically produce oligosaccharides with a DP up to 6 or 7 (5–7, 14). The production of relatively short oligosaccharides by *Nc*LPMO9C could be the result of a glucanase background activity in the enzyme sample or by *Nc*LPMO9C having activity on soluble oligosaccharides. Fig. 2*B* shows that *Nc*LPMO9C indeed is able to oxidatively degrade cello-oligosaccharides. The enzyme readily degraded Glc_5 and Glc_6, while showing lower activity on Glc_4 and no or minute activity on Glc_3. There is abundant evidence for these conversions being caused by *Nc*LPMO9C and not an impurity in the enzyme preparation: 1) the reaction generates oxidized species (see below for detailed characterization), 2) product formation was not observed in the absence of a reducing agent (results not shown), and 3) product formation was not observed in the presence of reducing agent only (results not shown). The oxidized products released were mainly DP2 from Glc_4 and Glc_5 and a mix of DP2 and DP3 from Glc_6 (Fig. 2*B*).

The degradation patterns shown in Fig. 2 (*A* and *B*) were independent of the reductant used (we tested hydroquinone, ascorbic acid, and catechin in concentrations varying from 1.5 to 10 mM). Fig. 2*B* (CDH trace) further shows that use of *Mt*CDH as electron donor for degradation of Glc_5 led to a clear change in the product profile. As expected, native oligosaccharides were no longer observed because they were oxidized to aldonic acids. The oxidized species observed between 26 and 29 min for the reactions with a reducing agent present were not seen, but a new peak appeared at ~40 min that may represent double oxidized species, an interpretation that is supported by mass spectrometry and NMR analysis of the samples (see below). This shift clearly shows that the products eluting between 25 and 30 min cannot be aldonic acids, because the CDH oxidizes reducing ends.

MS analysis confirmed the presence of only two major products upon incubating *Nc*LPMO9C with Glc_5, namely an oxidized dimer and a nonoxidized trimer (see below for details). Nevertheless, the chromatograms (Fig. 2) show additional peaks eluting in between the native and the main oxidized products. We propose that this is due to tautomerization, because keto groups on ring carbons are prone to this process at the elevated pH values used during the HPAEC runs. Migration of the 4-keto group to C3 and maybe C2 will change the elution behavior of the oligosaccharides.

*Nc*LPMO9C is the first LPMO unequivocally shown to be active on soluble cello-oligosaccharides. The fact that the pentamer is degraded faster than the tetramer and the clear preference for releasing an oxidized dimer from Glc_5 indicates the presence of at least five subsites on the enzyme running from −3 to +2 (subsites numbered according to the nomenclature used for glycoside hydrolases) (28). Degradation of Glc_6 yielded both DP2 and DP3 oxidized species, indicating binding to −4 to +2 and −3 to +3. Notably, the location of these subsites and

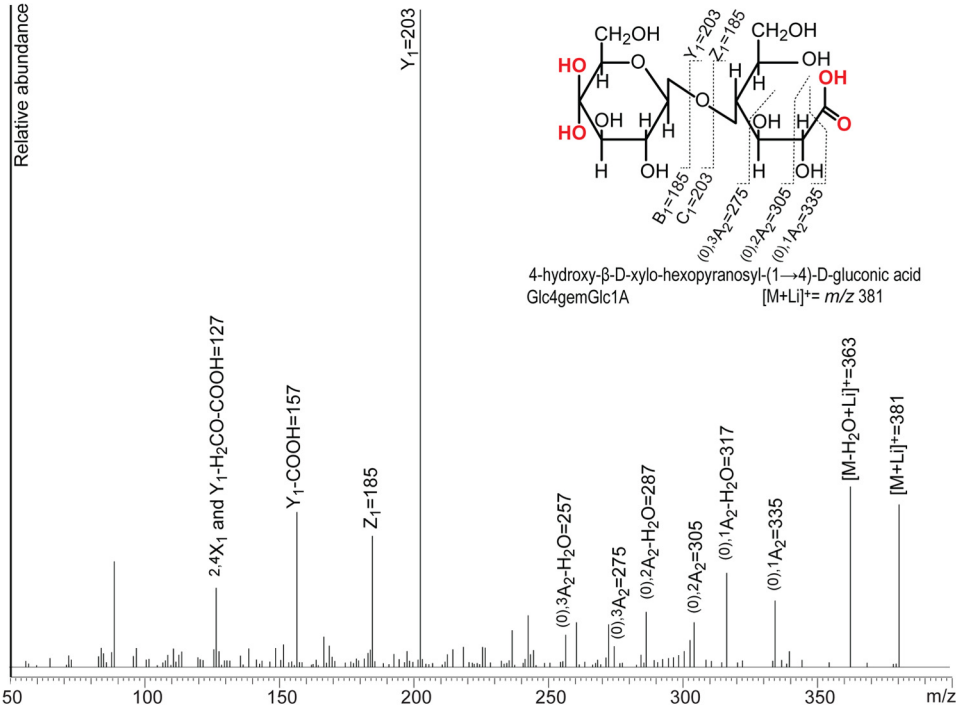

FIGURE 5. **MS/MS analysis of a double oxidized dimer (Glc4gemGlc1A) generated by treating cellopentaose with *Nc*LPMO9C and *Mt*CDH.** The analysis was done with lithium doping, and all labeled signals reflect lithium adducts.

the orientation of the productively bound substrate relative to the catalytic center are currently unknown.

To test whether the cello-oligosaccharide oxidizing activity of *Nc*LPMO9C is specific or an unspecific side reaction, the enzyme was incubated with other oligosaccharides (Man_6, Xyl_5, Xyl_6, chitopentaose, and maltodextrin) and both crystalline α-chitin and nanofibrillar α- and β-chitin. No activity was observed on any of these substrates. Thus, *Nc*LPMO9C seems to be specific for β-1–4-linked glucose units.

Product Identification by MS—MS analysis of product mixtures showed that the main products from degradation of Glc_5 were two species with *m*/*z* values of 527 and 381, corresponding to the sodium adducts of Glc_3 and a cellobiose with a gemdiol (*i.e.*, a hydrated keto group) at the nonreducing end, respectively. Minor amounts of cellobiose and oxidized cellotriose were also detected. To investigate this further, the time course of the enzyme reaction was studied in $H_2{}^{18}O$. This resulted in the same signal of *m*/*z* 527, whereas a new peak at *m*/*z* 383 appeared (Fig. 3*A*). This shows that the oxygen of the glycosidic linkage remains in the Glc_3 product as the OH group at C1, whereas the oxidized product acquires one oxygen atom from water and one from oxygen as schematically shown in Fig. 3*B*. As indicated in Fig. 3*A*, a *m*/*z* 385 peak appears after some time, which is due to the lactone-gemdiol equilibrium leading to exchange with water and, thus, to the eventual incorporation of two ^{18}O atoms.

Because the glycosidic bond in cello-oligosaccharides (and cellulose) links the C1 of one glucose to the C4 of the adjacent glucose, it is logical to suggest that the oxidation carried out by *Nc*LPMO9C takes place at the C4 position of the nonreducing end moiety. The resulting keto sugar will be in equilibrium with the C4 gemdiol in water solution (a feature that is common to keto saccharides (29)). Generally, it is not straightforward to prove the position of LPMO generated oxidations using mass spectrometry because the masses of various possible products are identical and because the mass difference between sodium and potassium adducts equals the mass of an oxygen atom. As shown in Fig. 1, the aldonic acid and gemdiol forms have identical masses, as do the corresponding lactone and keto forms. Thus, MS analysis alone cannot determine the type of LPMO activity. Exploiting the low complexity product mixtures obtainable thanks to the activity of *Nc*LPMO9C on soluble substrates, we have addressed this issue by carrying out MS/MS analyses of products after lithium doping, which facilitates reducing end cross-ring fragmentation (30), as well as by NMR analyses.

Fig. 4 shows the result of MS/MS analysis of the *m*/*z* 365 $[M+Li]^+$ products (oxidized dimers) generated by *Nc*LPMO9C and C1 oxidizing *Pc*LPMO9D (7). The spectra show differences including the occurrence of fragment ions that are diagnostic for C1 or C4 oxidations. Cellobionic acid (fragments indicated in *blue* in Fig. 4) readily loses mass corresponding to one carboxyl group (*m*/*z* 319). The C4 oxidized dimer (fragments indicated in *black* in Fig. 4) readily loses masses corresponding to both one and two water molecules (*m*/*z* 347 and 329) but does not generate ions corresponding to the loss of a carboxyl group. In addition, the most prevalent Y_1 and Z_1 ions (31) from glycosidic bond cleavage will be different for the two oxidized compounds. The Y_1 and Z_1 ions for glycosidic bond cleavage of cellobionic acid have *m*/*z* values of 203 and 185, respectively, species that include the carboxylic acid. The Y_1 and Z_1 ions for the C4 oxidized dimer have *m*/*z* values of 187 and 169, respectively, meaning no oxidation in the reducing end. The corresponding B_1 and C_1 ions (for the

TABLE 1

Fragmentation table for MS/MS analysis of native and oxidized cellobiose and cellotriose compounds

The table shows the *m/z* values of sodium and lithium adducts of the different fragments. n.a., not analyzed. # represents $[M+2Metal-H]^+$. Double ox represents a double oxidized oligosaccharide with a gemdiol in the nonreducing end and an aldonic acid in the downstream end. Fragmentation nomenclature according to Domon and Costello (31).

		Mother ions		Major fragments						
DP	Metal		$[M+metal]^+$	$-H_2O$	$-2H_2O$	B_1/B_2	C_1/C_2	Y_1/Y_2	Z_1/Z_2	–COOH
2	Na	Native	365	347	n.a	185	203	203	185	n.a
		–Glc1A	381	363	n.a	185	203	219	201	335
		–Glc1A #	403	385	n.a	207	225	241	223	357
		Glc4gem–	381	363	345	201	219	203	185	n.a
		Double ox	397	379	361	201	219	219	201	351
2	Li	Native	349	331	n.a	169	187	187	169	n.a
		–Glc1A	365	347	n.a	169	187	203	185	319
		–Glc1A #	371	353	n.a	175	193	209	191	325
		Glc4gem–	365	347	329	185	203	187	169	n.a
		Double ox	381	363	345	185	203	203	185	335
DP	Metal		$[M+metal]^+$	$-H_2O$	$-2H_2O$	B_1/B_2	C_1/C_2	Y_1/Y_2	Z_1/Z_2	–COOH
3	Na	Native	527	509	n.a	185/347	203/365	203/365	185/347	n.a
		–Glc1A	543	525	n.a	185/347	203/365	219/381	201/363	497
		–Glc1A #	565	547	n.a	207/369	225/387	241/403	223/385	519
		Glc4gem–	543	525	507	201/363	219/381	203/365	185/347	n.a
		Double ox	559	541	523	363	381	381	363	513
3	Li	Native	511	493	n.a	169/331	187/349	187/349	169/331	n.a
		–Glc1A	527	509	n.a	169/331	187/349	203/365	185/347	481
		–Glc1A #	533	515	n.a	175/337	193/355	209/371	191/353	487
		Glc4gem–	527	509	491	185/347	203/365	187/349	169/331	n.a
		Double ox	543	525	507	185/347	203/365	203/365	185/347	497

		Mother ions		Cross ring cleavages					
DP	Metal		$[M+metal]^+$	$^{0,2}A_2$	$^{2,4}A_2$	$^{3,5}A_2$	$^{0,2}X_1$	$^{2,4}X_1$	$^{3,5}X_1$
2	Na	Native	365	305	245	259	245	305	291
		–Glc1A	381	305	245	259	261	321	307
		–Glc1A #	403	327	267	281	283	343	329
		Glc4gem–	381	321	261	275	245	305	291
		Double ox	397	321	261	275	261	321	307
2	Li	Native	349	289	229	243	229	289	275
		–Glc1A	365	289	229	243	245	305	291
		–Glc1A #	371	295	235	249	251	311	297
		Glc4gem–	365	305	245	259	229	289	275
		Double ox	381	305	245	259	245	305	291
DP	Metal		$[M+metal]^+$	$^{0,2}A_2$	$^{2,4}A_2$	$^{3,5}A_2$	$^{0,2}X_2$	$^{2,4}X_2$	$^{3,5}X_2$	$^{0,2}A_3$	$^{2,4}A_3$	$^{3,5}A_3$	$^{0,2}X_3$	$^{2,4}X_3$	$^{3,5}X_3$
3	Na	Native	527	305	245	259	245	305	291	467	407	421	407	467	453
		–Glc1A	543	305	245	259	261	321	307	467	407	421	423	483	469
		–Glc1A #	565	327	267	281	283	343	329	489	429	443	445	505	491
		Glc4gem–	543	321	261	275	245	305	291	483	423	437	407	467	453
		Double ox	559	321	261	275	261	321	307	483	423	437	423	483	469
3	Li	Native	511	289	229	243	229	289	275	451	391	405	391	451	437
		–Glc1A	527	289	229	243	245	305	291	451	391	405	407	467	453
		–Glc1A #	533	295	235	249	251	311	297	457	397	411	413	473	459
		Glc4gem–	527	305	245	259	229	289	275	467	407	421	391	451	437
		Double ox	543	305	245	259	245	305	291	467	407	421	407	467	453

C4 oxidized dimer) are *m/z* 185 and 203, respectively, and tend to lose a water molecule, generating *m/z* 167 and 185 species, respectively. Loss of a water molecule from the B_1 and C_1 ions seems a likely event considering the presence of the gemdiol group at C4.

Notably, comparison of the *blue* and *black spectra* in Fig. 4 shows that MS/MS analysis can reveal whether an LPMO oxidizes the reducing or the nonreducing end of the substrate. Distinct *m/z* ions for cellobionic acid are 319, 203, and 157. For Glc4gemGlc, distinct *m/z* ions are 347, 329, and 287. A rela-

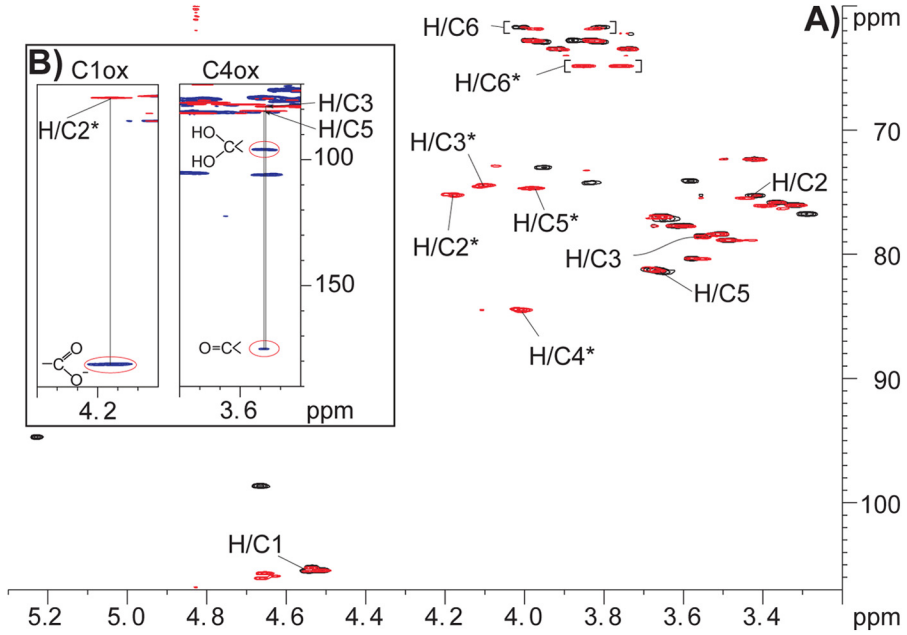

FIGURE 6. **NMR analysis of reaction products.** *A*, overlay of ^{13}C HSQC spectra for reaction products generated by treating 0.9 mg/ml cellopentaose with 2.9 μM *Nc*LPMO9C in the presence of 10 mM hydroquinone (black signals) or 0.9 μM *Mt*CDH (*red signals*). The samples were both in 99.996% D_2O with 5 mM sodium acetate, pH 6.0, and spectra were recorded at 25 °C. Peaks in the proton/carbon signals of the C4 oxidized monosaccharide residue are marked by H/C#, where # refers to the ring carbon number (overlapping *red* and black *signals*). Peaks in the proton/carbon signals of the C1 oxidized monosaccharide residue are marked by H/C#* (only *red signals*). For the sake of simplicity, peaks related to nonoxidized monosaccharide residues are not marked (a full assignment of chemical shifts is provided in Table 2). *B*, two details of an overlay of a ^{13}C HSQC spectrum and a ^{13}C HMBC spectrum recorded for products obtained in a reaction with both *Nc*LPMO9C and CDH. The *left panel* shows a correlation (indicated by a *vertical line*) from the H/C2* peak in HSQC (*red*) to a peak with a carbon chemical shift of 181.1 ppm in HMBC (*blue*), corresponding well to the (expected) presence of a carboxylate group at position C1. The *right panel* shows correlation from the H/C3 and H/C5 peaks in HSQC (*red*) to carbon peaks with a carbon chemical shift at C4 of 95.9 and 175.2 ppm in HMBC (*blue*), corresponding to the presence of a gemdiol and a keto group at C4, respectively.

tively high *m*/*z* 187 signal is also typical for Glc4gemGlc. In the case CDH is used as the electron donor for a C4-oxidizing LPMO, double oxidized products will emerge (Fig. 2*B*, *CDH trace*) with yet another characteristic MS/MS pattern, as illustrated in Fig. 5. Lithium and sodium adducts of MS/MS fragments obtained for the different LPMO products are summarized in Table 1.

Product Identification by NMR—To obtain proof for the identity of the oxidized reaction products, NMR spectroscopy was used to analyze products generated from cellopentaose by *Nc*LPMO9C in the presence of either CDH or hydroquinone (Fig. 6). The individual monosaccharide residues were assigned by starting at the anomeric signal and/or at the primary alcohol group at C6 and then following the proton-proton connectivity using TOCSY, DQF-COSY/IP-COSY, and ^{13}C HSQC-[^{1}H,^{1}H]TOCSY, whereas connectivity between the individual monosaccharide residues was obtained from the HMBC spectrum (see Table 2 for assignment of chemical shifts). These experiments showed the presence of dimeric and trimeric products in both reactions, as expected from the MS analyses described above. An overlay of the ^{13}C HSQC spectra of product mixtures obtained in the presence of hydroquinone or CDH (Fig. 6*A*) readily shows different occurrence of oxidations. C4 oxidation occurs in both reactions, whereas signals reflecting C1 oxidation are only observed in the reaction with CDH (*red signals* in Fig. 6*A*). There were no indications of oxidation of C6 because this part of the ^{13}C HSQC spectrum was essentially identical to that observed for nontreated cellopentaose and because no novel signals possibly reflecting additional oxidations were observed.

^{13}C HMBC spectra provided further insight into the nature of the products. This is illustrated by Fig. 6*B*, showing an overlay of the ^{13}C HSQC and the ^{13}C HMBC spectra of products obtained in the reaction with *Nc*LPMO9C and CDH. The overlay shows correlations from H/C-5 and H/C-3 to peaks with a carbon chemical shift at C4 of 95.9 and 175.2 ppm, corresponding well to the chemical shift of a gemdiol (29) and keto group, respectively. The gemdiol and keto groups account for ~80 and 20% of the signal intensity, respectively. Although documentation on the keto:gemdiol ratio in literature is limited, the gemdiol would be expected to dominate at pH 6.0 because the keto group is easily hydrated (29) in aqueous medium. The overlay also shows a correlation from the H/C-2 to a peak with a carbon chemical shift of 181.1 ppm that corresponds well to the shift expected when a carboxylate group is present at position C1 (12). Even though there are two different Glc1A groups in the product mixture (one in a trimeric and one in a dimeric product), their chemical shifts are very similar, meaning that the peaks appear nearly at the same position in the spectra, looking like one broad peak (see Table 2 for more details). Thus, for the first time, NMR has been used to prove that the products generated by a nonreducing end active LPMO are oxidized in the C4 position and that the products primarily exist as a gemdiol.

Suppression of H_2O_2 Production—In the absence of a cellulosic substrate, activated LPMOs produce H_2O_2 (17). We employed this ability to demonstrate binding of cello-oligo-

TABLE 2

Assignment of chemical shifts

The individual monosaccharide residues were assigned by starting at the anomeric signal and/or at the primary alcohol group at C6 and then following the proton-proton connectivity using TOCSY, DQF-COSY/IP-COSY, and ^{13}C HSQC-TOCSY spectra. ^{13}C HSQC was used for assigning the carbon chemical shifts. The ^{13}C HMBC spectrum provided long range bond correlations, allowing identification of the connectivity between the sugar units and allowing identification of the carboxyl group at C1, as well as the gem-diol group and keto group at C4. Chemical shifts were assigned for the major products resulting from treatment of 0.9 mg/ml cellopentaose with 2.9 μM *Nc*LPMO9C in the presence of 0.9 μM *Mt*CDH or 10 mM hydroquinone in 99.996% D_2O with 5 mM sodium acetate pD 6.0, for spectra recorded at 25 °C. Numbers 1–6 represent ring carbon numbers to which the chemical shift values (^1H, ^{13}C or ^1H, ^1H, ^{13}C for C6) are assigned for a nonreducing end glucose (NR), a second after NR glucose (SNR), the α anomer of glucose (α), the β anomer of glucose (β), the aldonate glucose (C1), and the keto/gemdiol glucose (C4). The chemical shifts reported are with accuracy of 0.01 ppm for ^1H and 0.1 ppm for ^{13}C, based on spectral resolution.

Glucose unit/carbon number	1	2	3	4	5	6
Hydroquinone, Glc_3						
NR	4.51; 105.4	3.32; 76.0	3.49; 78.6	3.51; 78.4	3.42; 72.3	3.93; 3.73; 63.5
SNR	4,54; 105.1	3.37; 75.8	3.67; 77.0	3.62; 81.2	3.61; 77.7	3.97; 3.83; 62.8
α	5.22; 94.7	3.57; 74.1	3.83; 74.1	3.65; 81.5	3.95; 73.0	3.96; 3.83; 62.8
β	4.66; 98.6	3.29; 76.8	3.65; 77.6	3.61; 81.3	3.63; 77.1	3.98; 3.87; 62.8
Hydroquinone, Glc4gemGlc						
C4	4.55; 105.5	3.41; 75.3	3.55; 78.5	175.2/95.9	3.58; 80.4	4.02; 3.81; 61.7
α	5.22; 94.7	3.57; 74.1	3.83; 74.1	3.65; 81.5	3.95; 73.0	3.96; 3.83; 62.8
β	4.66; 98.6	3.29; 76.8	3.65; 77.6	3.61; 81.3	3.63; 77.1	3.98; 3.87; 62.8
***Mt*CDH, Glc_2Glc1A**						
NR	4.51; 105.3	3.32; 76.1	3.42; 78.4	3.50; 78.3	3.49; 72.3	3.91; 3.74; 63.4
SNR	4.65; 105.6	3.41; 76.1	3.66; 76.9	3.67; 81.4	3.60; 77.8	3.97; 3.82; 62.8
C1	181.1	4.18; 75.2	4.10; 74.4	4.01; 84.51	3.99; 74.7	3.85; 3.76; 64.8
***Mt*CDH, Glc4gemGlc1A**						
C4	4.53; 105.3	3.44; 75.5	3.55; 78.6	175.2/95.9	3.65; 80.3	3.82; 3.98; 61.8
C1	181.1	4.18; 75.2	4.10; 74.4	4.01; 84.51	3.99; 74.7	3.85; 3.76; 64.8

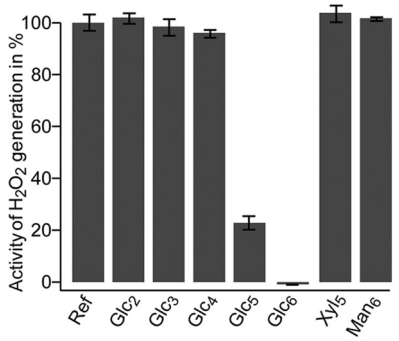

FIGURE 7. **Generation of H_2O_2 by *Nc*LPMO9C.** The enzyme was incubated with reductant and the production of H_2O_2 (here referred to as activity) was measured as described under "Experimental Procedures." The figure shows that the enzyme generates H_2O_2 in the absence of oligosaccharides (*Ref*) and in the presence of Xyl_5, Man_6, or short cello-oligosaccharides, whereas cello-oligosaccharide with DP > 4 diminish H_2O_2 production, indicative of productive binding to the LPMO. The reported results are mean values of five experiments. Control experiments without the reductant or the LPMO showed no H_2O_2 production, regardless of the presence of cello-oligosaccharides.

meric substrates to *Nc*LPMO9C. Fig. 7 shows that production of H_2O_2 was diminished in the presence of cello-oligosaccharides with a DP >4. Although only minor inhibition was observed in the presence of Glc_4, almost complete inhibition of H_2O_2 formation was observed in the presence of Glc_6. Thus, the data in Fig. 7 show that cello-oligomers with a minimal length of five sugars form complexes with the enzyme that are sufficiently strong to suppress the futile H_2O_2 generating side reaction. This corresponds very well with the HPLC data, which showed high activity for Glc_5 and Glc_6 and much lower activity for Glc_4 (Fig. 2*B*). As mentioned above, *Nc*LPMO9C is not active on Xyl_5 or Man_6, and Fig. 7 shows that these substrates do not suppress the H_2O_2 production.

Sequence and Structural Model of NcLPMO9C—For comparison, the sequence of *Nc*LPMO9C was aligned to a C1 oxidizing and a nonreducing end oxidizing LPMO. The AA9 domain of *Nc*LPMO9C shares 36.6% sequence identity with C1-oxidizing *Pc*LPMO9D (7) and 47.5% with nonreducing end oxidizing *Nc*LPMO9D (8, 16) (Fig. 8*A*). The metal coordinating residues (His-1 and His-83 in *Nc*LPMO9C) as well as four residues surrounding the copper site (Asn-26, His-155, Gln-164, and Tyr-166 in *Nc*LPMO9C) are conserved in all three AA9s. Looking at the LPMO structures available, AA9s tend to contain several surface-exposed aromatic residues that seem to be aligned to interact with a cellulose chain that would then traverse the catalytic center (32). Indeed, these aromatic residues have roughly the same spatial orientation as residues that, by experiment, have been shown to interact with chitin in an AA10 LPMO (33). This adds confidence to the notion that these aromatic residues interact with the substrate, possibly analogous to what is been suggested for *Pc*LPMO9D (32).

Based on the crystal structure of *Nc*LPMO9D a model was built for *Nc*LPMO9C. Comparison of the surface-exposed residues potentially involved in substrate binding (Fig. 8*B*) shows that there are more aromatic residues on the surfaces of *Nc*LPMO9D and *Pc*LPMO9D compared with *Nc*LPMO9C. Because of this difference, the length of the substrate-binding surface seems shorter in *Nc*LPMO9C. Even if one considers the contribution of protruding polar residues on the surface, the binding surface of *Nc*LPMO9C seems less extended (Fig. 8*B*) and possibly more adapted to binding shorter substrates compared with *Pc*LPMO9D and *Nc*LPMO9D. Interestingly, the structural model of *Nc*LPMO9C indicates that this enzyme has a cluster of three asparagine residues (Asn-25, Asn-26, and Asn-27) in a location that could potentially be a +2 subsite. One could speculate that these asparagines interact with the reducing end sugar. Indeed, as illustrated in Fig. 8*B*, a cellopentaose would span the putative binding surface of *Nc*LPMO9C, when its reducing end is positioned near these asparagines. Such an orientation would be in accordance with the observation that cellopentaose primarily is cleaved into a cellotriose and a Glc4gemGlc.

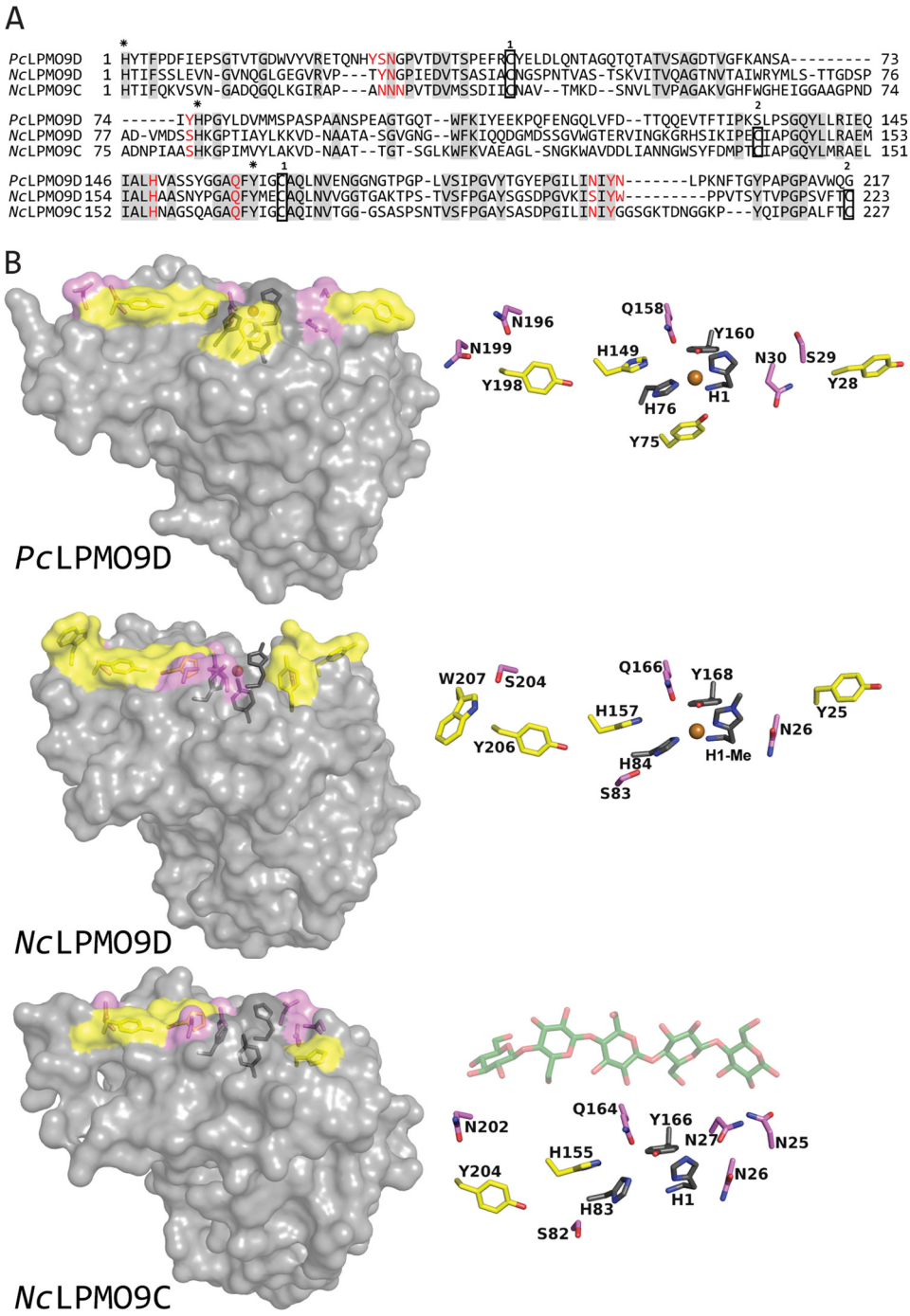

FIGURE 8. **Sequence and structural comparisons of *Pc*LPMO9D, *Nc*LPMO9D and *Nc*LPMO9C.** *A*, structure-guided sequence alignment of *Pc*LPMO9D, *Nc*LPMO9D, and *Nc*LPMO9C with fully conserved residues shaded in *gray*. Residues involved in coordination of the copper are marked with *asterisks* above the sequence (His-1, His-83 and Tyr-166 in *Nc*LPMO9C), whereas aromatic surface residues and protruding polar surface residues potentially involved in substrate binding are colored in red (all highlighted in *B*). Cysteines forming disulfide bonds are indicated in *boxes* with *numbers* above showing which cysteines are connected. *B*, side chains on the substrate binding surface of *Pc*LPMO9D (Protein Data Bank code 4B5Q) and *Nc*LPMO9D (Protein Data Bank code 4EIR) compared with the modeled structure of *Nc*LPMO9C. Copper coordinating residues are colored *dark gray*, aromatic and protruding polar residues putatively involved in substrate binding are colored *yellow* and *violet*, respectively, and the copper is shown as an *orange sphere*. For illustration purposes only, a cellopentaose (coordinates derived from Protein Data Bank code 2EEX; shown in *green* with oxygens in *red*) is placed above the surface of the modeled structure of *Nc*LPMO9C. The view in the *right panels* is rotated 90° relative to the view in the *left panels*, looking down at the flat surface containing the copper binding site.

Conclusions—In this article, we have shown that *Nc*LPMO9C cleaves both crystalline cellulose as well as cello-oligosaccharides yielding products oxidized in the nonreducing end. By applying NMR, we unambiguously showed that the nonreducing end sugar was oxidized at the C4 position and that this sugar primarily exists as a gemdiol in solution. We have also shown that MS/MS fragmentation analysis of oxidized products can be applied to differentiate between C1 and C4 oxidizing LMPOs. A range of different substrates were tested, but *Nc*LPMO9C was only active on β-1,4-linked glucose units, and the enzyme

seemed to require a minimum stretch of at least four glucose units. It has not escaped our attention that such an activity on short cello-oligosaccharides could imply that the enzyme is active on hemicellulose structures containing β-1,4-linked glucose units.

Acknowledgments—We thank Prof. Johannes Vliegenthart and Dr. Derek Horton for suggesting IUPAC nomenclature for the enzyme products. We thank Morten Skaugen for help in managing our HPLC and MS systems.

REFERENCES

1. Horn, S. J., Vaaje-Kolstad, G., Westereng, B., and Eijsink, V. G. (2012) Novel enzymes for the degradation of cellulose. *Biotechnol. Biofuels* **5,** 45
2. Cantarel, B. L., Coutinho, P. M., Rancurel, C., Bernard, T., Lombard, V., and Henrissat, B. (2009) The carbohydrate-active enzymes database (CAZy). An expert resource for glycogenomics. *Nucleic Acids Res.* **37,** D233–D238
3. Levasseur, A., Drula, E., Lombard, V., Coutinho, P. M., and Henrissat, B. (2013) Expansion of the enzymatic repertoire of the CAZy database to integrate auxiliary redox enzymes. *Biotechnol. Biofuels* **6,** 41
4. Vaaje-Kolstad, G., Westereng, B., Horn, S. J., Liu, Z., Zhai, H., Sørlie, M., and Eijsink, V. G. (2010) An oxidative enzyme boosting the enzymatic conversion of recalcitrant polysaccharides. *Science* **330,** 219–222
5. Forsberg, Z., Vaaje-Kolstad, G., Westereng, B., Bunæs, A. C., Stenstrøm, Y., MacKenzie, A., Sørlie, M., Horn, S. J., and Eijsink, V. G. (2011) Cleavage of cellulose by a CBM33 protein. *Protein Sci.* **20,** 1479–1483
6. Quinlan, R. J., Sweeney, M. D., Lo Leggio, L., Otten, H., Poulsen, J. C., Johansen, K. S., Krogh, K. B., Jørgensen, C. I., Tovborg, M., Anthonsen, A., Tryfona, T., Walter, C. P., Dupree, P., Xu, F., Davies, G. J., and Walton, P. H. (2011) Insights into the oxidative degradation of cellulose by a copper metalloenzyme that exploits biomass components. *Proc. Natl. Acad. Sci. U.S.A.* **108,** 15079–15084
7. Westereng, B., Ishida, T., Vaaje-Kolstad, G., Wu, M., Eijsink, V. G., Igarashi, K., Samejima, M., Ståhlberg, J., Horn, S. J., and Sandgren, M. (2011) The putative endoglucanase PcGH61D from *Phanerochaete chrysosporium* is a metal-dependent oxidative enzyme that cleaves cellulose. *PLoS One* **6,** e27807
8. Phillips, C. M., Beeson, W. T., Cate, J. H., and Marletta, M. A. (2011) Cellobiose dehydrogenase and a copper-dependent polysaccharide monooxygenase potentiate cellulose degradation by *Neurospora crassa*. *ACS Chem. Biol.* **6,** 1399–1406
9. Langston, J. A., Shaghasi, T., Abbate, E., Xu, F., Vlasenko, E., and Sweeney, M. D. (2011) Oxidoreductive cellulose depolymerization by the enzymes cellobiose dehydrogenase and glycoside hydrolase 61. *Appl. Environ. Microbiol.* **77,** 7007–7015
10. Sygmund, C., Kracher, D., Scheiblbrandner, S., Zahma, K., Felice, A. K., Harreither, W., Kittl, R., and Ludwig, R. (2012) Characterization of the two *Neurospora crassa* cellobiose dehydrogenases and their connection to oxidative cellulose degradation. *Appl. Environ. Microbiol.* **78,** 6161–6171
11. Hemsworth, G. R., Taylor, E. J., Kim, R. Q., Gregory, R. C., Lewis, S. J., Turkenburg, J. P., Parkin, A., Davies, G. J., and Walton, P. H. (2013) The copper active site of CBM33 polysaccharide oxygenases. *J. Am. Chem. Soc.* **135,** 6069–6077
12. Westereng, B., Agger, J. W., Horn, S. J., Vaaje-Kolstad, G., Aachmann, F. L., Stenstrøm, Y. H., and Eijsink, V. G. (2013) Efficient separation of oxidized cello-oligosaccharides generated by cellulose degrading lytic polysaccharide monooxygenases. *J. Chromatogr. A* **1271,** 144–152
13. Bey, M., Zhou, S., Poidevin, L., Henrissat, B., Coutinho, P. M., Berrin, J.-G., and Sigoillot, J.-C. (2013) Cello-oligosaccharide oxidation reveals differences between two lytic polysaccharide monooxygenases (Family GH61) from *Podospora anserina*. *Appl. Environ. Microbiol.* **79,** 488–496
14. Beeson, W. T., Phillips, C. M., Cate, J. H., and Marletta, M. A. (2012) Oxidative cleavage of cellulose by fungal copper-dependent polysaccharide monooxygenases. *J. Am. Chem. Soc.* **134,** 890–892
15. Tian, C., Beeson, W. T., Iavarone, A. T., Sun, J., Marletta, M. A., Cate, J. H., and Glass, N. L. (2009) Systems analysis of plant cell wall degradation by the model filamentous fungus *Neurospora crassa*. *Proc. Natl. Acad. Sci. U.S.A.* **106,** 22157–22162
16. Li, X., Beeson, W. T., 4th, Phillips, C. M., Marletta, M. A., and Cate, J. H. (2012) Structural basis for substrate targeting and catalysis by fungal polysaccharide monooxygenases. *Structure* **20,** 1051–1061
17. Kittl, R., Kracher, D., Burgstaller, D., Haltrich, D., and Ludwig, R. (2012) Production of four *Neurospora crassa* lytic polysaccharide monooxygenases in *Pichia pastoris* monitored by a fluorimetric assay. *Biotechnol. Biofuels* **5,** 79
18. Zámocký, M., Schumann, C., Sygmund, C., O'Callaghan, J., Dobson, A. D., Ludwig, R., Haltrich, D., and Peterbauer, C. K. (2008) Cloning, sequence analysis and heterologous expression in *Pichia pastoris* of a gene encoding a thermostable cellobiose dehydrogenase from *Myriococcum thermophilum*. *Protein Expr. Purif.* **59,** 258–265
19. Flitsch, A., Prasetyo, E. N., Sygmund, C., Ludwig, R., Nyanhongo, G. S., and Guebitz, G. M. (2013) Cellulose oxidation and bleaching processes based on recombinant *Myriococcum thermophilum* cellobiose dehydrogenase. *Enzyme Microb. Technol.* **52,** 60–67
20. Harreither, W., Sygmund, C., Augustin, M., Narciso, M., Rabinovich, M. L., Gorton, L., Haltrich, D., and Ludwig, R. (2011) Catalytic properties and classification of cellobiose dehydrogenases from Ascomycetes. *Appl. Environ. Microbiol.* **77,** 1804–1815
21. Wood, T. M. (1988) Preparation of crystalline, amorphous, and dyed cellulase substrates. *Methods Enzymol.* **160,** 19–25
22. Ifuku, S., and Saimoto, H. (2012) Chitin nanofibers. Preparations, modifications, and applications. *Nanoscale* **4,** 3308–3318
23. Xia, Y., Legge, G., Jun, K. Y., Qi, Y., Lee, H., and Gao, X. (2005) IP-COSY, a totally in-phase and sensitive COSY experiment. *Magn. Reson. Chem.* **43,** 372–379
24. Armougom, F., Moretti, S., Poirot, O., Audic, S., Dumas, P., Schaeli, B., Keduas, V., and Notredame, C. (2006) Expresso. Automatic incorporation of structural information in multiple sequence alignments using 3D-coffee. *Nucleic Acids Res.* **34,** W604–W608
25. Söding, J., Biegert, A., and Lupas, A. N. (2005) The HHpred interactive server for protein homology detection and structure prediction. *Nucleic Acids Res.* **33,** W244–W248
26. Sali, A., and Blundell, T. L. (1993) Comparative protein modelling by satisfaction of spatial restraints. *J. Mol. Biol.* **234,** 779–815
27. Kitago, Y., Karita, S., Watanabe, N., Kamiya, M., Aizawa, T., Sakka, K., and Tanaka, I. (2007) Crystal structure of Cel44A, a glycoside hydrolase family 44 endoglucanase from *Clostridium thermocellum*. *J. Biol. Chem.* **282,** 35703–35711
28. Davies, G. J., Wilson, K. S., and Henrissat, B. (1997) Nomenclature for sugar-binding subsites in glycosyl hydrolases. *Biochem. J.* **321,** 557–559
29. Kopper, S., and Freimund, S. (2003) The composition of keto aldoses in aqueous solution as determined by NMR spectroscopy. *Helv. Chim. Acta* **86,** 827–843
30. Cancilla, M. T., Wong, A. W., Voss, L. R., and Lebrilla, C. B. (1999) Fragmentation reactions in the mass spectrometry analysis of neutral oligosaccharides. *Anal. Chem.* **71,** 3206–3218
31. Domon, B., and Costello, C. E. (1988) A systematic nomenclature for carbohydrate fragmentations in FAB-MS/MS spectra of glycoconjugates. *Glycoconj. J.* **5,** 397–409
32. Wu, M., Beckham, G. T., Larsson, A. M., Ishida, T., Kim, S., Payne, C. M., Himmel, M. E., Crowley, M. F., Horn, S. J., Westereng, B., Igarashi, K., Samejima, M., Ståhlberg, J., Eijsink, V. G., and Sandgren, M. (2013) Crystal structure and computational characterization of the lytic polysaccharide monooxygenase GH61D from the basidiomycota fungus *Phanerochaete chrysosporium*. *J. Biol. Chem.* **288,** 12828–12839
33. Aachmann, F. L., Sørlie, M., Skjåk-Braek, G., Eijsink, V. G., and Vaaje-Kolstad, G. (2012) NMR structure of a lytic polysaccharide monooxygenase provides insight into copper binding, protein dynamics, and substrate interactions. *Proc. Natl. Acad. Sci. U.S.A.* **109,** 18779–18784